LANGMUIR

pubs.acs.org/Langmuir Article

Determination of Critical Micelle Concentration from the Diffusion-Driven Dilution of Micellar Aqueous Mixtures

Eliandreina Cruz Barrios and Onofrio Annunziata*

Cite This: *Langmuir* 2021, 37, 2855−2862 Read Online

ACCESS | Metrics & More | Article Recommendations

ABSTRACT: Micellization is a phenomenon of central importance in surfactant solutions. Here, we demonstrate that the diffusion-based spreading of the free boundary between a micellar aqueous solution and pure water yields a one-dimensional spatial profile of surfactant concentration that can be used to identify the critical micelle concentration, here denoted as C^*. This can be achieved because dilution of micelles into water leads to their dissociation at a well-defined position along the concentration profile and an abrupt increase in the diffusion coefficient. Rayleigh interferometry was successfully employed to determine C^* values for three well-known surfactants in water at 25 °C: Triton X-100 (TX-100), sodium dodecyl sulfate (SDS), and poly(oxyethylene)(4)Lauryl Ether (Brij-30). The dependence of C^* on salt concentration was also characterized for TX-100 in the presence of Na_2SO_4, NaCl, and NaSCN. Accurate values of C^* can be directly identified by visual inspection of the corresponding concentration-gradient profiles. To apply the method of least squares to experimental concentration profiles, a mathematical expression was derived from Fick's law and the pseudophase separation model of micellization with the inclusion of appropriate modifications. While Rayleigh interferometry was employed in our experiments, this approach can be extended to any experimental technique that yields one-dimensional profiles of surfactant concentration. Moreover, diffusion-driven surfactant disaggregation is precise, noninvasive, requires single-sample preparation, and applies to both nonionic and ionic surfactants. Thus, this work provides the foundation of diffusion-driven dilution methods, thereby representing a valuable addition to existing techniques for the determination of C^*.

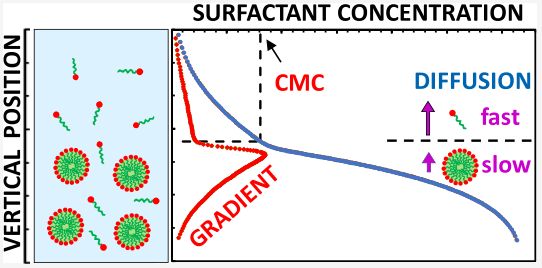

INTRODUCTION

Surfactants are organic molecules with a nonpolar chain covalently linked to a polar or ionic molecular group. In aqueous solutions, their amphiphilic property leads to a reversible self-associative process denoted as micellization.[1,2] This process typically produces globular nanoaggregates known as micelles, with the nonpolar hydrophobic chains forming the core of the micelle and the hydrophilic groups positioned at the micelle−water interface, thereby optimizing micelle interaction with its surrounding fluid. Since the hydrophobic core of micelles can host hydrophobic molecules, surfactant aqueous solutions have been of paramount importance for their broad-spectrum of applications in drug solubilization,[3,4] drug delivery,[3,5] detergency,[6] catalysis,[7] protein crystallization and purification,[8] soil remediation,[9] and enhanced oil recovery.[10,11]

Although micelles are water-soluble aggregates, a micellar solution can be described as a heterogeneous mixture in which micelles are regarded as a second pseudophase, well dispersed within a solvent medium. As in the case of solute crystal solubility in solution, the formation of micelles can be thought to occur only above a characteristic surfactant concentration known as critical micelle concentration, here denoted as C^*. This phase-transition description of micellization is appropriate not only because of micelle mesoscopic size but also because of the cooperative and reversible nature of micelle formation.[12,13]

The C^* value of a surfactant plays a crucial role in characterizing and optimizing the thermodynamic stability of micelles and solubilization of drugs, substrates, or petroleum-related compounds.[12−14] Thus, the experimental determination of C^* values has always been a primary goal of surfactant characterizations.[12,15−26] Historically, C^* values have been determined from the plot of a solution's physical property such as surface tension, changes in absorbance or fluorescence upon dye solubilization, turbidity, colligative properties, equivalent conductivity, self-diffusion, nuclear-magnetic, and electron-paramagnetic resonance.[27−36] Related techniques usually require multiple-sample preparation and analysis; some are restricted to ionic surfactants or involve the use of probes. Due to limitations of individual methods and the urgency of

Received: January 19, 2021
Revised: February 7, 2021
Published: February 17, 2021

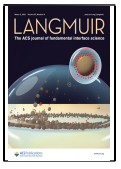

https://dx.doi.org/10.1021/acs.langmuir.1c00176
Langmuir 2021, 37, 2855−2862

surfactant characterizations, there is a continuous demand for the development of new methods for rapid and precise C^* determination.[14−26] Here, we demonstrate that the diffusion-driven dilution of micelles into a solvent can be used to observe disaggregation at a well-defined location. Specifically, we show that the diffusion-based spreading of the boundary between a micellar aqueous solution and pure water yields a one-dimensional spatial profile of surfactant concentration that can be then used to identify the value of C^*. Bearing in mind that the accuracy of C^* is related to the validity of the phase-transition approximation, this approach is precise, noninvasive, applicable to both ionic and nonionic surfactants, and yields C^* values from single experiments without the need for multiple-sample preparation.

In the present work, we use precision Rayleigh interferometry, which gives the one-dimensional refractive-index profile inside a vertical channel in which a surfactant solution is interfaced with its solvent.[37,38] We determine C^* for three well-known surfactants in water at 25 °C. These surfactants are Triton X-100 (TX-100), as an example of nonionic surfactant (C^* = 0.23−0.24 mM, ≈0.15 g·L^{-1}),[39−41] sodium dodecyl sulfate (SDS), as an example of ionic surfactant (C^* = 7.6−8.4 mM, ≈2.3 g·L^{-1}),[39,41,42] and poly(oxyethylene)(4)Lauryl Ether (Brij-30) to examine method sensitivity as this nonionic surfactant has a significantly low C^* value (0.039−0.085 mM, ≈0.02 g·L^{-1}).[39,43,44] An important problem in the field of surfactants is to examine the effect of additives on physicochemical properties such as micellization and cloud point.[45] In our case, we characterized the dependence of C^* on salt type and concentration in the case of TX-100 to examine method precision. Indeed, salts do not strongly affect the C^* value of nonionic surfactants compared to the case of ionic surfactants, for which C^* significantly decreases due to a common-ion effect.[46] Salt studies are also relevant to the Hofmeister series, which traditionally ranks salt ions according to their ability in reducing protein solubility and increasing the stability of protein folded state. A similar ranking was also found to apply to synthetic polymers and surfactants.[47−49]

THEORY

In this section, the basic theory demonstrating why diffusion-based boundary spreading can be used to determine C^* values is outlined. Specifically, the one-dimensional concentration profile, $C(x,t)$, produced by the isothermal diffusion-based spreading of the boundary between a micellar aqueous solution of concentration $C = C_{max}$ (with $C_{max} > C^*$) and water ($C = 0$) is theoretically examined, with x and t being the position perpendicular to boundary and time, respectively. To derive the theoretical expression of $C(x,t)$, we apply the pseudophase separation model to a nonionic surfactant. Micelle dissociation is expected to be sufficiently fast that can be assumed to instantaneously occur[50] as surfactant concentration becomes lower than C^* due to dilution.

According to Fick's first law of diffusion, the mutual-diffusion coefficient, D, for a surfactant−water mixture, is given by[50,51]

$$D = \left(\frac{dC_S}{dC}\right)D_S + \left(\frac{dC_M}{dC}\right)D_M \tag{1}$$

where D_S and D_M are the free surfactant (unimer) and micelle diffusion coefficients, respectively. We shall assume that these two parameters are constant and identifiable with the corresponding tracer-diffusion coefficients, with D_M significantly smaller than D_S due to the relatively large hydrodynamic radius of micelles compared to free surfactant unimers.[49] Correspondingly, C_S and C_M are the surfactant concentrations in the unimer and micellar states, with $C = C_S + C_M$ being the total surfactant concentration. According to eq 1, D is a weighted average of D_S and D_M, with the derivatives, dC_S/dC and dC_M/dC, being the corresponding weights. These total derivatives originate from the concentration gradients of individual species.

According to the pseudophase separation model,[13] we have $C_M = 0$ and $C_S = C$ for $C < C^*$, and $C_M = C−C^*$ and $C_S = C^*$ for $C > C^*$. Hence, eq 1 can be rewritten as follows

$$D = D_S\,H(C^* - C) + D_M\,H(C - C^*) \tag{2}$$

where $H(z)$ is the Heaviside step function with $H(z) = 0$ and 1 when $z < 0$ and $z > 0$, respectively. Based on this description, the mutual-diffusion coefficient of a surfactant−water system exhibits a jump discontinuity point at the critical micelle concentration.[50−53] This behavior is distinct from that of the self-diffusion coefficient, $D^{(s)} = (C_S/C)D_S + (C_M/C)D_M$,[27,34,54] which remains continuous at $C = C^*$ because it is a weighted average based on species concentrations instead of their derivatives as shown in eq 1.

Concentration profiles $C(x,t)$ are extracted from Fick's second law.[55] According to eq 2, this can be written in the following way

$$\frac{\partial C}{\partial t} = D_S\frac{\partial^2 C}{\partial x^2} \quad (C<C^*) \tag{3a}$$

$$\frac{\partial C}{\partial t} = D_M\frac{\partial^2 C}{\partial x^2} \quad (C>C^*) \tag{3b}$$

The general solution of eqs 3a and 3b is given by[55]

$$C = A + B\,\mathrm{erf}(D_S^{-1/2}y) \quad (C<C^*) \tag{4a}$$

$$C = A' + B'\,\mathrm{erf}(D_M^{-1/2}y) \quad (C > C^*) \tag{4b}$$

where $y \equiv (1/2)xt^{-1/2}$ is the reduced position, $\mathrm{erf}(z) \equiv (2\pi^{-1/2})\cdot\int_0^z e^{-s^2}\,ds$ is the error function, and A, B, A', and B' are constants to be determined. If we set $C = 0$ and C_{max} at $y = -\infty$ and $+\infty$, respectively (free-boundary condition[37,55]), we deduce that $A - B = 0$ and $A' + B' = C_{max}$. Thus, eqs 4a and 4b become

$$C = A\,[1 + \mathrm{erf}(D_S^{-1/2}y)] \quad (C < C^*) \tag{5a}$$

$$C = A' + (C_{max} - A')\,\mathrm{erf}(D_M^{-1/2}y) \quad (C > C^*) \tag{5b}$$

To identify A and A', we observe that $C = C^*$ corresponds to a unique reduced position, y^*, attainable from both eqs 5a and 5b, with $y \le y^*$ and $y \ge y^*$ corresponding to $C \le C^*$ and $C \ge C^*$, respectively. Thus, by applying the continuity condition of $C = C^*$ at $y = y^*$ to eqs 5a and 5b, we obtain

$$C = \left[\frac{1 + \mathrm{erf}(D_S^{-1/2}y)}{1 + \mathrm{erf}(D_S^{-1/2}y^*)}C^*\right]H(C^* - C) + \left[C_{max} - \frac{1 - \mathrm{erf}(D_M^{-1/2}y)}{1 - \mathrm{erf}(D_M^{-1/2}y^*)}(C_{max} - C^*)\right]H(C - C^*) \tag{6}$$

https://dx.doi.org/10.1021/acs.langmuir.1c00176
Langmuir 2021, 37, 2855−2862

Note that the behavior of $C(y)$ described by eq 6 is equivalent to that predicted for the diffusion of a solute through two different media interfaced at y^*.[55] However, the position, y^*, is typically known in this mass transfer problem, contrary to our case.

After choosing values of C^*, D_M, and D_S, eq 6 can be used to generate the theoretical profiles of surfactant concentration, $C(y)$, provided that y^* is also known. The value of y^* can be linked to that of C^* assuming that diffusion flux, J, is also a continuous function at $y = y^*$ due to mass conservation

$$J|_{y\to y^{*-}} = J|_{y\to y^{*+}} \tag{7}$$

To obtain the explicit form of eq 7, the two limiting expressions of the concentration gradient, dC/dx at $y \to y^{*-}$ and $y \to y^{*+}$, can be deduced from eq 6

$$\left.\frac{dC}{dx}\right|_{y\to y^{*-}} = (\pi t)^{-1/2}\frac{{D_S}^{-1/2}\, e^{-y^{*2}/D_S}}{1 + \mathrm{erf}({D_S}^{-1/2}y^*)}C^* \tag{8a}$$

$$\left.\frac{dC}{dx}\right|_{y\to y^{*+}} = (\pi t)^{-1/2}\frac{{D_M}^{-1/2} e^{-y^{*2}/D_M}}{1 - \mathrm{erf}({D_M}^{-1/2}y^*)}(C_{max} - C^*) \tag{8b}$$

After inserting eqs 8a and 8b into Fick's first law, $J = -D\cdot dC/dx$,[56] with $D = D_S$ for $y = y^{*-}$ and $D = D_M$ for $y = y^{*+}$, eq 7 yields the following relation between C^* and y^*

$$\frac{C^*}{C_{max} - C^*} = \left(\frac{D_M}{D_S}\right)^{1/2}\frac{1 + \mathrm{erf}({D_S}^{-1/2}y^*)}{1 - \mathrm{erf}({D_M}^{-1/2}y^*)}\, e^{-({D_M}^{-1} - {D_S}^{-1})y^{*2}} \tag{9}$$

It is important to observe that the values of y cannot be experimentally identified prior to C^* determination. Indeed, the reference position of $y = 0$ varies with respect to that fixed by an external reference frame, depending on the value of C^*/C_{max}. It is therefore convenient to introduce the experimentally accessible position, Y, with the reference value of $Y = 0$ always corresponding to the profile midpoint at $C = C_{max}/2$. Correspondingly, we replace y with $Y + y_c$ in eq 6, with y_c being the value of y at $C = C_{max}/2$. The value of y_c can be linked to that of y^* after substituting $C = C_{max}/2$ in eq 6. If experiments are designed such that $C_{max}/2 > C^*$, we have

$$\mathrm{erf}({D_M}^{-1/2}y_c) = 1 - \frac{1 - \mathrm{erf}({D_M}^{-1/2}y^*)}{2(1 - C^*/C_{max})} \tag{10}$$

In summary, eq 6 shows the link between the surfactant concentration profile caused by diffusion-based boundary spreading and C^*. While $C(y)$ is a continuous function, this model predicts that its first derivative, dC/dy, displays a discontinuity point at $y = y^*$ due to the sharp change in diffusion coefficient (see eq 2) at this location.

EXPERIMENTAL SECTION

Materials. Triton X-100 (TX-100; 647 g·mol^{-1}) and polyoxyethylene(4)Lauryl Ether (Brij-30; 362.55 g·mol^{-1}) were obtained from Sigma-Aldrich. Sodium dodecyl sulfate (SDS; 288.37 g·mol^{-1}) Sodium chloride (NaCl; 58.44 g·mol^{-1}), sodium sulfate (Na_2SO_4; 142.04 g·mol^{-1}), and sodium thiocyanate (NaSCN; 81.07 g·mol^{-1}) were obtained from Merck. Sodium thiocyanate was heated in an oven at 100 °C for 7 h and kept in a desiccator. The other materials were used as received without further purification. Deionized water was passed through a four-stage Millipore filter system to provide high-purity water for all of the experiments. In the case of Na_2SO_4, a binary salt−water stock solution was prepared due to salt hygroscopicity. Its composition was determined from density measurements and the known density-composition relation.[57] All other solutions were prepared by weight using a Mettler-Toledo AT400 analytical balance. Molar concentrations were obtained from the density of solutions and reported molecular weights. All density measurements were made with a Mettler-Paar DMA40 density meter, thermostated with water from a large, well-regulated (±0.001 °C) water bath.

Boundary-Spreading Experiments. All diffusion-based boundary-spreading experiments were made with the high-precision Gosting diffusiometer operated in its Rayleigh interferometric optical mode.[37,38,58−61] A boundary-spreading experiment begins with the preparation of a sharp boundary (using a peristaltic pump) between a surfactant−water solution and water inside a vertical channel of a Tiselius cell. For experiments with TX-100 in the presence of salts, a surfactant−salt−water solution is interfaced with a salt−water solution at the same salt concentration. With the exception of the Brij-30 case, all surfactant aqueous solutions exhibit higher density than the corresponding surfactant-free solutions, and they are therefore located at the bottom of the vertical channel to prevent convection. As diffusion occurs, boundary broadening occurs. Experiments are completed before the boundary spreads throughout the diffusion channel so that the compositions at the two-channel extremities remain the same within the experimental error and the free-boundary condition applies. The light source used for generating the Rayleigh interference pattern is a He−Ne Uniphase laser with wavelength λ = 543.5 nm. A cell holder is located inside a water bath. The temperature of the bath was regulated (±0.001 °C) at 25.00 °C. The cell holder has the function to support a Tiselius cell, where diffusion occurs, and a mask, which consists of a double window. Here, the laser beam is split into two parts: one going through the diffusion channel of the Tiselius cell and one passing through the water bath (reference channel). A pair of two-cylinder lenses focus the diffusion channel onto the detector, where the Rayleigh interference pattern is observed and recorded. If a homogeneous liquid (solution or water) occupies the entire diffusion channel, then a set of vertical parallel Rayleigh fringes will be generated. For fluids with a vertically nonuniform concentration, Rayleigh fringes shift horizontally as the refractive index inside the diffusion channel changes with vertical height. This gives direct information about the refractive index versus vertical position and leads to the determination of the surfactant concentration profile, as discussed below.

Data from the Rayleigh interference patterns were collected with a linear charge-coupled device (CCD) array (6000 pixels, 10 μm × 10 μm pixels), mounted vertically on a precision stage. For a given experiment, at least 10 interference patterns were collected at different times. For a given interference pattern, vertical positions along the recorded pattern were converted into the actual positions inside the diffusion channel, X, using the known magnification factor of 1.7108. Vertical positions were then converted into the corresponding reduced positions, $Y \equiv X\cdot(2t)^{-1/2}$, where t is the time at which the position was recorded after the experiment start. The stage with this vertical array was stepped horizontally through the two-dimensional interference pattern to collect the data necessary to characterize a surfactant concentration profile. Data acquisition was controlled via computer, which also performed the subsequent data reduction. If one starts from a fringe location corresponding to the surfactant-free solution ($C = 0$) inside the diffusion channel and vertically moves toward the surfactant solution ($C = C_{max}$) through the pattern, the horizontal shift of the fringe can be determined until becomes as large as the distance between two adjacent fringes. At this vertical position, one fringe is crossed. As the location of the initial surfactant solution is finally reached ($C = C_{max}$), a total of $\mathcal{J}$ fringes will be crossed. Note that the total number of fringes, $\mathcal{J}$, is not an integer in general because it is directly proportional to the difference in refractive index between the surfactant solution and water. At a given reduced position, Y, a recorded fringe shift, j, is given by the sum of the number of fringes crossed and the fractional shift of a fringe. The vertical position associated with $j = \mathcal{J}/2$ is set to correspond to $Y = 0$.

https://dx.doi.org/10.1021/acs.langmuir.1c00176
Langmuir 2021, 37, 2855−2862

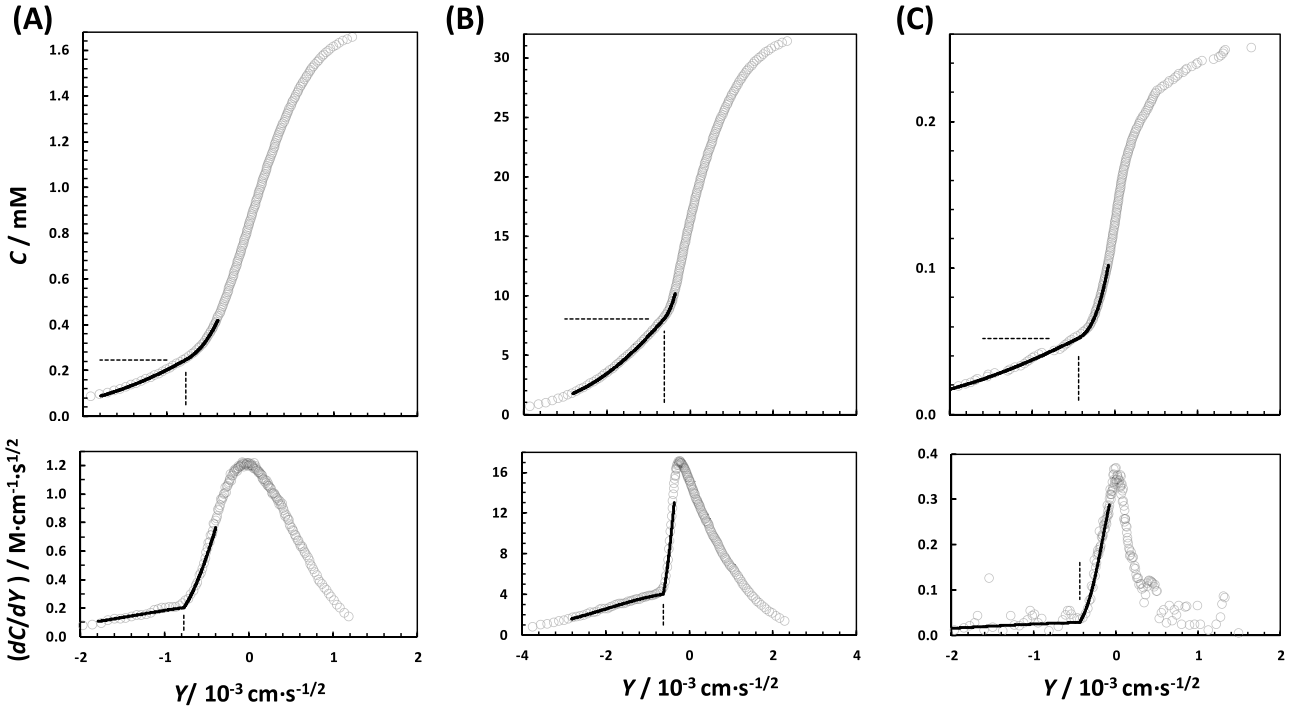

Figure 1. Sigmoidal concentration profiles, $C(Y)$, characterizing boundary spreading between a surfactant−water solution and water at 25 °C for TX-100 (A), SDS (B), and Brij-30 (C). Bottom figures show the corresponding profiles of the concentration gradient, dC/dY. Vertical dashed lines locate Y^*, while the corresponding horizontal dashed lines locate C^*. Solid curves are fit through the experimental data, which are discussed in the Results and Discussion section.

To extract the corresponding surfactant concentration profile, $C(Y)$, we set $C/C_{max} = j/\mathcal{J}$ at any given Y. In other words, we assume that the solution refractive index is a linear function of surfactant concentration. This is an approximation since the refractive-index contribution of a free surfactant molecule is slightly different from that of a micellar surfactant molecule.[53] Finally, in the case of ternary surfactant−salt−water mixtures, we assume that salt cross-diffusion[57] induced by the surfactant concentration gradient can be ignored. Both approximations are not expected to affect the determination of C^* within the method experimental error. An individual interference pattern obtained during a boundary-spreading experiment can be separately analyzed for the determination of C^*. Thus, the analysis of multiple interference patterns associated with a single experiment was used to extract the average and standard deviation of all C^* values extracted.

RESULTS AND DISCUSSION

Representative concentration profiles, $C(Y)$, characterizing boundary spreading between micellar aqueous solutions and water are illustrated in Figure 1A−C for TX-100, SDS, and Brij-30, respectively. The concentration gradients, dC/dY, were numerically deduced from the $C(Y)$ curves. These are shown under the corresponding concentration profiles.

In the absence of micelle dissociation, the $C(Y)$ sigmoidal curves are expected to be described by $C = (C_{max}/2)\cdot[1 + \mathrm{erf}(D_M^{-1/2}Y)]$.[55] Correspondingly, first derivatives should be described by a centrosymmetric Gaussian function: $dC/dY = C_{max}\cdot(\pi D_M)^{-1/2}\cdot\exp(-Y^2/D_M)$. Our experimental data of $C(Y)$ show a significant deviation from this behavior due to dilution-induced micelle dissociation. This deviation becomes especially noticeable when inspecting the corresponding dC/dY profiles. Here, we can observe an abrupt change in slope at a well-defined value of $Y = Y^*$. This is then used to identify the value of C^* for the surfactant in the corresponding $C(Y)$ curve (see dashed lines in Figure 1). Since experiments were designed such that $C^* < C_{max}/2$, Y^* is located on the left side of the maximum of dC/dY. Note that an inflection point occurs between Y^* and the location of the maximum at $Y \approx 0$.

Although the direct inspection of our experimental data is expected to give critical micelle concentrations by graphic interpolation, it is convenient to identify a mathematical expression that yields the value of C^* by applying the method of least squares to experimental data. Clearly, the theoretical model discussed in the Theory section represents the starting point of this analysis. However, dC/dY is predicted to exhibit a discontinuity point at $Y = Y^*$ according to the pseudophase separation model, in disagreement with the experimental behavior in Figure 1A−C. This deviation, which makes the direct application of eqs 6, 9, and10 to experimental data not practicable, is mainly related to a shortcoming of the pseudophase separation model. Indeed, it is expected that mass−action−law models[62] more realistically describe the behavior of the diffusion coefficient as a function of surfactant concentration around $Y = Y^*$. According to mass−action−law models, the diffusion coefficient $D(C)$ in eq 1 will exhibit an inflection point around $C = C^*$.[48−51] Correspondingly, the gradient, dC/dY, is expected to remain a continuous function at $Y = Y^*$. However, the implementation of these models significantly increases mathematical complexity, making them also impracticable for our data analysis. Furthermore, even with a hypothetically exact thermodynamic description of micellization, the corresponding model for $D(C)$ would remain approximate due to the assumption that D_S and D_M are constants, independent of concentration.[53] Finally, in the case of ionic surfactants, the presence of the counterion further increases model complexity due to the common-ion effect, electrostatic dragging effects, counterion partial binding to micelles, and electrostatic and electrophoretic interactions.[52,53]

https://dx.doi.org/10.1021/acs.langmuir.1c00176
Langmuir 2021, 37, 2855−2862

Since we are specifically interested in the determination of C^*, it is practically convenient to retain the pseudophase separation model for nonionic surfactants and introduce corrections that would make this model suitable for examining experimental data for both nonionic and ionic surfactants.

As a first modification to the pseudophase separation model, we impose that dC/dY is a continuous function at $Y = Y^*$. This is achieved by assuming that D is a continuous function at $C = C^*$ as expected from the chemical−equilibrium model. If we then set D to be the same at $y \to y^{*-}$ and $y \to y^{*+}$, eq 7 becomes a continuity condition for the concentration gradient: $dC/dy|_{y \to y^{*-}} = dC/dy|_{y \to y^{*+}}$, consistent with experimental behavior. Correspondingly, eq 9 must be replaced by

$$\frac{C^*}{C_{max} - C^*} = \left(\frac{D_M}{D_S}\right)^{-1/2} \frac{1 + \mathrm{erf}(D_S^{-1/2} y^*)}{1 - \mathrm{erf}(D_M^{-1/2} y^*)} e^{-(D_M^{-1} - D_S^{-1}) y^{*2}} \quad (11)$$

Figure 2 shows theoretical concentration profiles calculated from eq 6 with C^*/C_{max} =0.25 and D_S/D_M =10. For comparison, we have applied both eq 9 (dashed curves) and eq 11 (solid curves). We can see that $C(Y)$ for the modified pseudophase separation model smoothly changes around $Y = Y^*$. Correspondingly, dC/dY remains a continuous function at $Y = Y^*$. Note that the slope of dC/dY retains its discontinuity at $Y = Y^*$ as we can appreciate from the more rapid increase of dC/dY after $Y = Y^*$. Furthermore, we can see that an inflection point in the behavior of dC/dY occurs at $Y > Y^*$ followed by a maximum, in qualitative agreement with the experimental behavior in Figure 1A−C. On the other hand, the dC/dY curve generated from the basic pseudophase separation model exhibits a marked discontinuity at $Y = Y^*$ with dC/dY sharply increasing. Moreover, the slope of dC/dY (d^2C/dY^2) even switches sign from positive to negative as Y increases. Due to this discontinuity point, the behavior of dC/dY lacks the inflection and maximum points that emerged in the curve generated from the modified model.

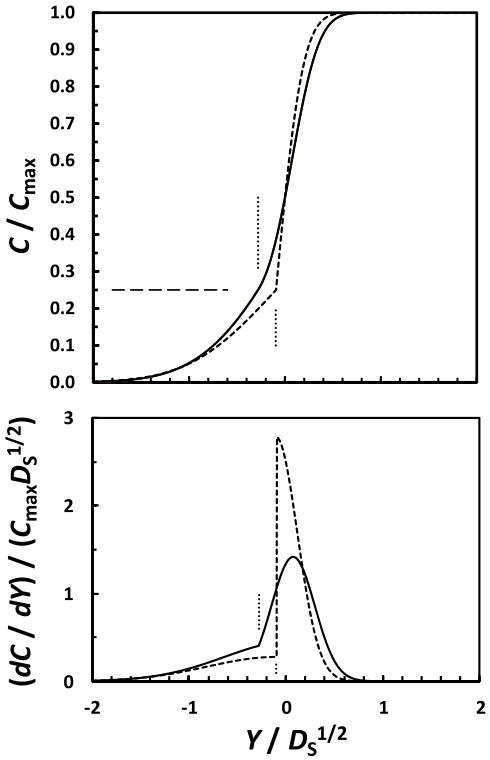

Figure 2. Theoretical concentration profile, $C(Y)$, extracted from eq 6 based on the modified model (eq 11; solid curve) with D_S/D_M = 10 and C^*/C_{max} = 0.25. For comparison, the corresponding concentration profile of the basic model (eq 9; dashed curve) is included. The bottom figure shows the corresponding profiles of the concentration gradient, dC/dY. Vertical dashed lines locate Y^*, while the corresponding horizontal dashed line locates C^*/C_{max}.

The proposed modification alone is not sufficient for a satisfactory application of the method of least squares to our data as it fails to correctly describe the magnitude and location of the experimental maximum of dC/dY. This failure is also caused by a concentration dependence of D_M, a problem that becomes especially important for ionic surfactants such as SDS. In this case, the counterion dragging effect on micelle diffusion, which is ignored in our model, makes micelle diffusion to significantly increase with surfactant concentration.[52,53] To overcome this issue, a second modification is introduced in the model by revisiting eq 10, which links y_c ($Y = 0$) to y^* ($Y = Y^*$). We specifically generalize eq 10 into

$$\mathrm{erf}(D_M^{-1/2} y_c) = 1 - \frac{1 - \mathrm{erf}(D_M^{-1/2} y^*)}{2\alpha(1 - C^*/C_{max})} \quad (12)$$

where we have introduced a new fitting parameter, α (with α = 1 in eq 10). Replacing eq 10 with eq 12 makes $C(Y)$ theoretical curves no longer satisfy the condition of $C = C_{max}/2$ at $Y = 0$ in general. Thus, we chose to apply the method of least squares to experimental values of $C(Y)$ on the left side of the maximum of dC/dY, ending around dC/dY inflection point as shown by the solid curves in Figure 1a−c. On the other hand, the lowest experimental value of $C(Y)$ to be examined was chosen to correspond to ≈5% of C_{max}, to reduce errors associated with experimental noise. Furthermore, this lower limit significantly reduces deviations of experimental data from the theoretical behavior of $C(Y)$ in the case of ionic surfactants, for which a strong concentration dependence of D_S at very low surfactant concentrations is known[53] to occur. In spite of these two chosen boundaries, the number of experimental data points to be analyzed around the critical micelle concentration remains large. Extracted values of C^* for the three investigated surfactants are reported in Table 1. These are in excellent agreement with the corresponding literature values[39−44] within the experimental error.

The precision of C^* data. (≈3% for TX-100) is sufficiently high that the effect of salt concentration and type on C^* could be successfully characterized in the case of nonionic TX-100. We have specifically considered the following three salts: Na_2SO_4, NaCl, and NaSCN due to their relevance to the Hofmeister series.[46−48] In this series, anions such as SO_4^{2-} display a great salting-out strength favoring the precipitation of water-soluble macromolecules such as proteins, whereas Cl^- is regarded as a mild anion located approximately at the midpoint of the Hofmeister series, separating salting-out from salting-in anions such as SCN^-. This ranking was also observed in the case of poly(ethylene glycol) (PEG) in water,[63,64] which represents the hydrophilic group of TX-100. However, PEG hydrophilic groups are not expected to undergo major environment changes upon micelle formation. Thus, salt effects should be mainly caused by ion interactions with hydrocarbon groups. Based on this argument, micelle disaggregation shares more similarity with protein unfolding.

https://dx.doi.org/10.1021/acs.langmuir.1c00176
Langmuir 2021, 37, 2855−2862

Table 1. Values of C* of Surfactant−Water Solutions at 25 °C

	C_{max}/mM	C*/mM
SDS	32.00	8.03 ± 0.06[a]
Brij-30	0.2551	0.051 ± 0.002
TX-100	1.689	0.236 ± 0.008
NaCl, 0.10 M[b]	1.716	0.211 ± 0.009
NaCl, 0.20 M	1.708	0.205 ± 0.005
NaCl, 0.30 M	1.705	0.199 ± 0.007
NaCl, 0.45 M	1.537	0.174 ± 0.009
Na_2SO_4, 0.05 M	1.681	0.205 ± 0.007
Na_2SO_4, 0.10 M	1.687	0.184 ± 0.005
Na_2SO_4, 0.20 M	1.670	0.154 ± 0.003
Na_2SO_4, 0.25 M	1.702	0.146 ± 0.003
Na_2SO_4, 0.30 M	1.640	0.139 ± 0.003
NaSCN, 0.20 M	1.690	0.247 ± 0.010
NaSCN, 0.30 M	1.694	0.232 ± 0.007
NaSCN, 0.40 M	1.700	0.231 ± 0.005
NaSCN, 0.50 M	1.711	0.238 ± 0.005

[a]Values of C* are averages of values extracted from different interference patterns. Corresponding errors are 2× standard deviations. [b]Salt names and concentrations refer to ternary TX-100 aqueous mixtures.

Here, anions such as SO_4^{2-} hinder protein unfolding and stabilize its native folded state while the SCN^- anion should favor unfolding.[49] For micelles, a salt-induced decrease in C* corresponds to an increase in micelle thermodynamic stability.[46]

Our experimental results of lnC* are plotted in Figure 3 as a function of osmolarity, $\nu_{SALT}C_{SALT}$, where ν_{SALT} is the number

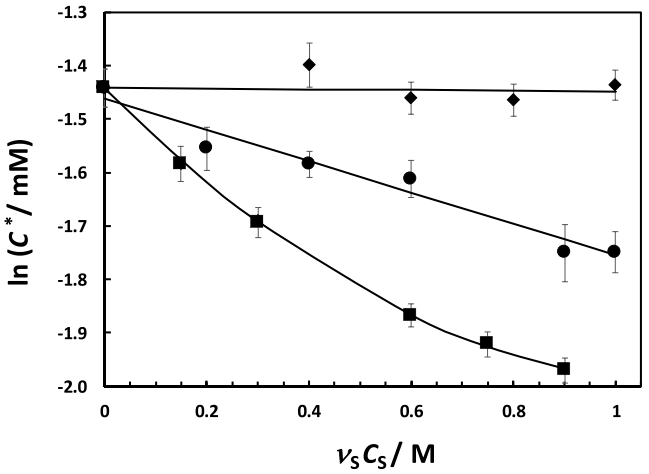

Figure 3. Logarithm of critical micelle concentration, lnC*, as a function of ion concentration, $\nu_{SALT}C_{SALT}$ for TX-100 at 25 °C in aqueous NaCl (circles), Na_2SO_4 (squares), and NaSCN (diamonds). Solid curves are fits through the experimental data.

of ions per formula unit and C_{SALT} is salt molar concentration. In the Na_2SO_4 and NaCl cases, lnC* decreases as ion concentration increases with the salting-out effect induced by Na_2SO_4 being about 3 times larger than that induced by NaCl. On the other hand, the effect of NaSCN on lnC* was found to be negligible within the experimental error. The determined effect of anion type on C*, which follows the Hofmeister series, is in good agreement with the literature.[46]

CONCLUSIONS

Experimental one-dimensional concentration profiles, $C(Y)$, characterizing the spreading of the boundary between micellar aqueous solutions and water were successfully characterized and analyzed for the determination of critical micelle concentrations, C*, in three surfactant cases (TX-100, SDS, and Brij-30). In the TX-100 case, $C(Y)$ was also characterized in the presence of a uniform salt concentration of Na_2SO_4, NaCl, and NaSCN. Values of C* can be identified by visual inspection of the corresponding concentration-gradient profiles, dC/dY (see Figure 1A−C). A theoretical expression of $C(Y)$ was developed by considering the pseudophase separation model for nonionic surfactants as a starting point. Modifications were then incorporated in the theoretical expression of $C(Y)$ allowing for limitations of the pseudophase separation model. This keeps mathematical complexity still adequate for applications to experimental data analysis of both nonionic and ionic surfactants using the method of least squares. Due to model shortcomings, C* values are expected to be method dependent. Nevertheless, they were found to fall within the range of C* data reported in the literature.[39−44] Within the framework of our method, the precision of the determined values of C* was found to be ≈3% and ≈0.01 g·L^{-1} represents the lowest value of C* that can be detected by Rayleigh interferometry based on Brij-30 results. While Rayleigh interferometry was employed for the characterization of $C(Y)$ in our experiments, concentration profiles can also be extracted using other techniques such as absorption spectroscopy. Thus, this work provides the foundation of diffusion-based methods for the determination of C*. These are noninvasive, require single-sample preparation, and apply to both nonionic and ionic surfactants.

AUTHOR INFORMATION

Corresponding Author

Onofrio Annunziata − *Department of Chemistry and Biochemistry, Texas Christian University, Fort Worth, Texas 76129, United States;* orcid.org/0000-0002-6636-4750; Email: o.annunziata@tcu.edu

Author

Eliandreina Cruz Barrios − *Department of Chemistry and Biochemistry, Texas Christian University, Fort Worth, Texas 76129, United States*

Complete contact information is available at: https://pubs.acs.org/10.1021/acs.langmuir.1c00176

Notes

The authors declare no competing financial interest.

ACKNOWLEDGMENTS

O.A. dedicates this article to the memory of Prof. Lucia Costantino Salerno who introduced him to the subjects of physical chemistry and surfactants. This work was supported by TCU Research and Creative Activity Funds.

REFERENCES

(1) Diamant, H.; Andelman, D. Free Energy Approach to Micellization and Aggregation: Equilibrium, Metastability, and Kinetics. *Curr. Opin. Colloid Interface Sci.* **2016**, *22*, 94−98.

(2) Lu, Y.; Zhang, E.; Yang, J.; Cao, Z. Strategies to Improve Micelle Stability for Drug Delivery. *Nano Res.* **2018**, *11*, 4985−4998.

(3) Singh, A. K.; Yadav, T. P.; Pandey, B.; Gupta, V.; Singh, S. P. Engineering Nanomaterials for Smart Drug Release. In *Applications of Targeted Nano Drugs and Delivery Systems*; Mohapatra, S. S.; Ranjan, S.; Dasgupta, N.; Mishra, R. K., Eds.; Elsevier: Amsterdam, 2019; pp 411−449.
(4) Gulyakin, I. D.; Oborotova, N. A.; Pechennikov, V. M. Solubilization of hydrophobic antitumor drugs. *Pharm. Chem. J.* **2014**, *48*, 209−213.
(5) Fuhrmann, K.; Schulz, J. D.; Gauthier, M. A.; Leroux, J.-C. PEG Nanocages as Non-Sheddable Stabilizers for Drug Nanocrystals. *ACS Nano* **2012**, *6*, 1667−1676.
(6) Yada, S.; Matsuoka, K.; Nagai Kanasaki, Y.; Gotoh, K.; Yoshimura, T. Emulsification, Solubilization, and Detergency Behaviors of Homogeneous Polyoxypropylene-Polyoxyethylene Alkyl Ether Type Nonionic Surfactants. *Colloids Surf., A* **2019**, *564*, 51−58.
(7) Li, J.; Tang, Y.; Wang, Q.; Li, X.; Cun, L.; Zhang, X.; Zhu, J.; Li, L.; Deng, J. Chiral Surfactant-Type Catalyst for Asymmetric Reduction of Aliphatic Ketones in Water. *J. Am. Chem. Soc.* **2012**, *134*, 18522−18525.
(8) Wong, F. W. F.; Ariff, A. B.; Stuckey, D. C. Downstream Protein Separation by Surfactant Precipitation: A Review. *Crit. Rev. Biotechnol.* **2018**, *38*, 31−46.
(9) Wang, M.; Zhang, B.; Li, G.; Wu, T.; Sun, D. Efficient Remediation of Crude Oil-Contaminated Soil Using a Solvent/Surfactant System. *RSC Adv.* **2019**, *9*, 2402−2411.
(10) Johannessen, A. M.; Spildo, K. Enhanced Oil Recovery (EOR) by Combining Surfactant with Low Salinity Injection. *Energy Fuels* **2013**, *27*, 5738−5749.
(11) Kamal, M. S. A Review of Gemini Surfactants: Potential Application in Enhanced Oil Recovery. *J. Surfactants Deterg.* **2016**, *19*, 223−236.
(12) Rosen, M. J.; Kunjappu, J. T. *Surfactants and Interfacial Phenomena*; John Wiley & Sons, Inc: Hoboken, 2012.
(13) Shinoda, K.; Hutchinson, E. Pseudo-Phase Separation Model for Thermodynamic Calculations on Micellar Solutions. *J. Phys. Chem. A.* **1962**, *66*, 577−582.
(14) Ottaviani, G.; Wendelspiess, S.; Alvarez-Sánchez, R. Importance of Critical Micellar Concentration for the Prediction of Solubility Enhancement in Biorelevant Media. *Mol. Pharm.* **2015**, *12*, 1171−1179.
(15) Zhu, Q.; Huang, L.; Su, J.; Liu, S. A Sensitive and Visible Fluorescence-Turn-on Probe for the CMC Determination of Ionic Surfactants. *Chem. Commun.* **2014**, *50*, 1107−1109.
(16) Cai, L.; Gochin, M.; Liu, K. A Facile Surfactant Critical Micelle Concentration Determination. *Chem. Commun.* **2011**, *47*, 5527.
(17) Fu, J.; Cai, Z.; Gong, Y.; O'Reilly, S. E.; Hao, X.; Zhao, D. A New Technique for Determining Critical Micelle Concentrations of Surfactants and Oil Dispersants via UV Absorbance of Pyrene. *Colloids Surf., A* **2015**, *484*, 1−8.
(18) Yu, D.; Huang, F.; Xu, H. Determination of Critical Concentrations by Synchronous Fluorescence Spectrometry. *Anal. Methods* **2012**, *4*, 47−49.
(19) Li, N.; Luo, H.; Liu, S. A New Method for the Determination of the Critical Micelle Concentration of Triton X-100 in the Absence and Presence of β-Cyclodextrin by Resonance Rayleigh Scattering Technology. *Spectrochim. Acta, Part A* **2004**, *60*, 1811−1815.
(20) Lin, C.-E. Determination of Critical Micelle Concentration of Surfactants by Capillary Electrophoresis. *J. Chromatogr. A* **2004**, *1037*, 467−478.
(21) Karimi, M. A.; Mozaheb, M. A.; Hatefi-Mehrjardi, A.; Tavallali, H.; Attaran, A. M.; Shamsi, R. A New Simple Method for Determining the Critical Micelle Concentration of Surfactants Using Surface Plasmon Resonance of Silver Nanoparticles. *J. Anal. Sci. Technol.* **2015**, *6*, No. 214.
(22) Tan, C. H.; Huang, Z. J.; Huang, X. G. Rapid Determination of Surfactant Critical Micelle Concentration in Aqueous Solutions Using Fiber-Optic Refractive Index Sensing. *Anal. Biochem.* **2010**, *401*, 144−147.
(23) Topel, Ö.; Çakır, B. A.; Budama, L.; Hoda, N. Determination of Critical Micelle Concentration of Polybutadiene-Block-Poly(ethyleneoxide) Diblock Copolymer by Fluorescence Spectroscopy and Dynamic Light Scattering. *J. Mol. Liq.* **2013**, *177*, 40−43.
(24) Salem, J. K.; El-Nahhal, I. M.; Najri, B. A.; Hammad, T. M. Utilization of Surface Plasmon Resonance Band of Silver Nanoparticles for Determination of Critical Micelle Concentration of Cationic Surfactants. *Chem. Phys. Lett.* **2016**, *664*, 154−158.
(25) Davis, B. M.; Richens, J. L.; O'Shea, P. Label-Free Critical Micelle Concentration Determination of Bacterial Quorum Sensing Molecules. *Biophys. J.* **2011**, *101*, 245−254.
(26) Nakahara, Y.; Kida, T.; Nakatsuji, Y.; Akashi, M. New Fluorescence Method for the Determination of the Critical Micelle Concentration by Photosensitive Monoazacryptand Derivatives. *Langmuir* **2005**, *21*, 6688−6695.
(27) Holmberg, K.; Jönsson, B.; Kronberg, B.; Lindman, B. *Surfactants and Polymers in Aqueous Solution*, 2nd ed.; John Wiley & Sons, Inc.: Hoboken, 2002.
(28) Mukherjee, I.; Moulik, S. P.; Rakshit, A. K. Tensiometric Determination of Gibbs Surface Excess and Micelle Point: A Critical Revisit. *J. Colloid Interface Sci.* **2013**, *394*, 329−336.
(29) Elworthy, P. H.; Mysels, K. J. The Surface Tension of Sodium Dodecylsulfate Solutions and the Phase Separation Model of Micelle Formation. *J. Colloid Interface Sci.* **1966**, *21*, 331−347.
(30) Patist, A.; Bhagwat, S. S.; Penfield, K. W.; Aikens, P.; Shah, D. O. On the Measurement of Critical Micelle Concentrations of Pure and Technical-Grade Nonionic Surfactants. *J. Surfactants Deterg.* **2000**, *3*, 53−58.
(31) Chatterjee, A.; Moulik, S. P.; Sanyal, S. K.; Mishra, B. K.; Puri, P. M. Thermodynamics of Micelle Formation of Ionic Surfactants: A Critical Assessment for Sodium Dodecyl Sulfate, Cetyl Pyridinium Chloride and Dioctyl Sulfosuccinate (Na Salt) by Microcalorimetric, Conductometric, and Tensiometric Measurements. *J. Phys. Chem. B* **2001**, *105*, 12823−12831.
(32) Garcia-Mateos, I.; Mercedes Velazquez, M.; Rodriguez, L. J. Critical Micelle Concentration Determination in Binary Mixtures of Ionic Surfactants by Deconvolution of Conductivity/Concentration Curves. *Langmuir* **1990**, *6*, 1078−1083.
(33) Kjellin, U. R. M.; Reimer, J.; Hansson, P. An Investigation of Dynamic Surface Tension, Critical Micelle Concentration, and Aggregation Number of Three Nonionic Surfactants Using NMR, Time-Resolved Fluorescence Quenching, and Maximum Bubble Pressure Tensiometry. *J. Colloid Interface Sci.* **2003**, *262*, 506−515.
(34) Söderman, O.; Stilbs, P.; Price, W. S. NMR Studies of Surfactants. *Concepts Magn. Reson., Part A* **2004**, *23*, 121−135.
(35) Vitiello, G.; Ciccarelli, D.; Ortona, O.; D'Errico, G. Microstructural Characterization of Lysophosphatidylcholine Micellar Aggregates: The Structural Basis for Their Use as Biomembrane Mimics. *J. Colloid Interface Sci.* **2009**, *336*, 827−833.
(36) Tedeschi, A. M.; Busi, E.; Paduano, L.; Basosi, R.; D'Errico, G. Influence of the Headgroup Molecular Structure on the Anionic surfactant−PVP Interaction Studied by Electron Paramagnetic Resonance of a Cationic Nitroxide. *Phys. Chem. Chem. Phys.* **2003**, *5*, 5077−5083.
(37) Miller, D. G.; Albright, J. G. Optical Methods. In *Measurement of the Transport Properties of Fluids: Experimental Thermodynamics*; Wakeham, W. A.; Nagashima, A.; Sengers, J. V., Eds.; Blackwell Scientific Publications: Oxford, U.K., 1991; *Vol. III*, pp 272−294.
(38) Annunziata, O.; Buzatu, D.; Albright, J. G. Protein Diffusion Coefficients Determined by Macroscopic-Gradient Rayleigh Interferometry and Dynamic Light Scattering. *Langmuir* **2005**, *21*, 12085−12089.
(39) Mukerjee, P.; Mysels, K. J. Critical Micelle Concentrations of Aqueous Surfactant Systems. *J. Pharm. Sci.* **1972**, *61*, 319.
(40) Tiller, G. E.; Mueller, T. J.; Dockter, M. E.; Struve, W. G. Hydrogenation of Triton X-100 Eliminates Its Fluorescence and Ultraviolet Light Absorption While Preserving Its Detergent Properties. *Anal. Biochem.* **1984**, *141*, 262−266.

https://dx.doi.org/10.1021/acs.langmuir.1c00176
Langmuir 2021, 37, 2855−2862

(41) Owoyomi, O.; Jide, I.; Akanni, M. S.; Soriyan, O. O.; Morakinyo, M. K. Interactions Between Sodium Dodecylsulphate and Triton X-100: Molecular Properties and Kinetics Investigations. *J. Appl. Sci.* **2005**, *5*, 729−734.
(42) Cifuentes, A.; Bernal, J. L.; Diez-Masa, J. C. Determination of Critical Micelle Concentration Values Using Capillary Electrophoresis Instrumentation. *Anal. Chem.* **1997**, *69*, 4271−4274.
(43) Bandyopadhyay, P.; Ghosh, A. K.; Bandyopadhyay, S. Brij-Micelle and Polyacrylic Acid Interaction Investigated by Cu2+-Induced Pyrene Fluorescence: Effect of Brij-Micelle Structure. *Chem. Phys. Lett.* **2009**, *476*, 244−248.
(44) Tripathi, S.; Brown, D. G. Effects of Linear Alkylbenzene Sulfonate on the Sorption of Brij 30 and Brij 35 onto Aquifer Sand. *Environ. Sci. Technol.* **2008**, *42*, 1492−1498.
(45) Rosen, M. J. *Surfactants and Interfacial Phenomena*, 3rd ed.; John Wiley & Sons: Hoboken, 2004.
(46) Ray, A.; Nemethy, G. Effects of Ionic Protein Denaturants on Micelle Formation by Nonionic Detergents. *J. Am. Chem. Soc.* **1971**, *93*, 6787−6793.
(47) Song, J.; Franck, J.; Pincus, P.; Kim, M. W.; Han, S. Specific Ions Modulate Diffusion Dynamics of Hydration Water on Lipid Membrane Surfaces. *J. Am. Chem. Soc.* **2014**, *136*, 2642−2649.
(48) Hao, L.-S.; Yang, N.; Xu, G.-Y.; Jia, Y.-F.; Liu, Q.; Nan, Y.-Q. Specific Ion Effects on the Micellization of Aqueous Mixed Cationic/Anionic Surfactant Systems with Various Counterions. *Colloids Surf., A* **2016**, *504*, 161−173.
(49) Zhang, Y.; Furyk, S.; Bergbreiter, D. E.; Cremer, P. S. Specific Ion Effects on the Water Solubility of Macromolecules: PNIPAM and the Hofmeister Series. *J. Am. Chem. Soc.* **2005**, *127*, 14505−14510.
(50) Weinheimer, R. M.; Evans, D. F.; Cussler, E. Diffusion in Surfactant Solutions. *J. Colloid Interface Sci.* **1981**, *80*, 357−368.
(51) Paduano, L.; Sartorio, R.; Vitagliano, V.; Costantino, L. Equilibrium and Transport Properties of Aqueous Pentaethyleneglycol-1-Hexyl Ether and Sodium Hexanesulfonate at 25 °C. *J. Colloid Interface Sci.* **1997**, *189*, 189−198.
(52) Leaist, D. O. Binary Diffusion of Micellar Electrolytes. *J. Colloid Interface Sci.* **1986**, *111*, 230−239.
(53) Annunziata, O.; Costantino, L.; D'Errico, G.; Paduano, L.; Vitagliano, V. Transport Properties for Aqueous Solution of Sodium Sulfonate Surfactants: 1. Mutual Diffusion Measurements: Evaluation of the Equilibrium Parameters for the Micellization Process. *J. Colloid Interface Sci.* **1999**, *216*, 8−15.
(54) Annunziata, O.; Costantino, L.; D'Errico, G.; Paduano, L.; Vitagliano, V. Transport Properties for Aqueous Sodium Sulfonate Surfactants: 2. Intradiffusion Measurements: Influence of the Obstruction Effect on the Monomer and Micelle Mobilities. *J. Colloid Interface Sci.* **1999**, *216*, 16−24.
(55) Crank, J. *The Mathematics of Diffusion*, 2nd ed.; Oxford University Press: Oxford, 1975.
(56) Cussler, E. L. *Diffusion: Mass Transfer in Fluid Systems*; Cambridge University Press: Cambridge, 1997.
(57) Rard, J. A.; Albright, J. G.; Miller, D. G.; Zeidler, M. E. Ternary Mutual Diffusion Coefficients and Densities of the System {z1NaCl +(1 −z1)Na2SO4}(aq) at 298.15 K and a Total Molarity of 0.5000 Mol dm−3. *J. Chem. Soc., Faraday Trans.* **1996**, *92*, 4187−4197.
(58) Annunziata, O.; Vergara, A.; Paduano, L.; Sartorio, R.; Miller, D. G.; Albright, J. G. Quaternary Diffusion Coefficients in a Protein−Polymer−Salt−Water System Determined by Rayleigh Interferometry. *J. Phys. Chem. B* **2009**, *113*, 13446−13453.
(59) Zhang, H.; Annunziata, O. Effect of Macromolecular Polydispersity on Diffusion Coefficients Measured by Rayleigh Interferometry. *J. Phys. Chem. B* **2008**, *112*, 3633−3643.
(60) Zhang, H.; Annunziata, O. Modulation of drug transport properties by multicomponent diffusion in surfactant aqueous solutions. *Langmuir* **2008**, *24*, 10680−10687.
(61) Tyrrell, H. J. V.; Harris, K. R. *Diffusion in Liquids*; Butterworths: London, 1984.
(62) Rusanov, A. I. The Mass-Action-Law Theory of Micellization Revisited. *Langmuir* **2014**, *30*, 14443−14451.
(63) McAfee, M. S.; Annunziata, O. Effects of Salting-In Interactions on Macromolecule Diffusiophoresis and Salt Osmotic Diffusion. *Langmuir* **2015**, *31*, 1353−1361.
(64) McAfee, M. S.; Zhang, H.; Annunziata, O. Amplification of Salt-Induced Polymer Diffusiophoresis by Increasing Salting-Out Strength. *Langmuir* **2014**, *30*, 12210−12219.

https://dx.doi.org/10.1021/acs.langmuir.1c00176
Langmuir 2021, 37, 2855−2862